Journal of Solid State Chemistry 184 (2011) 2818–2823

Contents lists available at SciVerse ScienceDirect

Journal of Solid State Chemistry

journal homepage: www.elsevier.com/locate/jssc

# Formation of β-nickel hydroxide plate-like structures under mild conditions and their optical properties

A.P. de Moura [a], R.C. Lima [b,*], E.C. Paris [c], M.S. Li [d], J.A. Varela [a], E. Longo [a]

[a] Universidade Estadual Paulista, Instituto de Química, CEP 14800-900 Araraquara, SP, Brazil
[b] Universidade Federal de Uberlândia, Instituto de Química, CEP 38400-902 Uberlândia, MG, Brazil
[c] Embrapa, Empresa Brasileira de Pesquisas Agropecuárias, CEP 13560-970 São Carlos, SP, Brazil
[d] Universidade de São Paulo, Instituto de Física de São Carlos, CEP 13566590 São Carlos, SP, Brazil

ARTICLE INFO

*Article history:*
Received 6 May 2011
Received in revised form
14 August 2011
Accepted 22 August 2011
Available online 26 August 2011

*Keywords:*
β-$Ni(OH)_2$ nanoplates
Microwave–hydrothermal
Growth mechanism
Rietveld refinement
Photoluminescence property

ABSTRACT

Nanostructural β-nickel hydroxide (β-$Ni(OH)_2$) plates were prepared using the microwave–hydrothermal (MH) method at a low temperature and short reaction times. An ammonia solution was employed as the coordinating agent, which reacts with $[Ni(H_2O)_6]^{2+}$ to control the growth of β-$Ni(OH)_2$ nuclei. A trigonal β-$Ni(OH)_2$ single phase was observed by X-ray diffraction (XRD) analyses, and the crystal cell was constructed with structural parameters and atomic coordinates obtained from Rietveld refinement. Field emission scanning electron microscopy (FE-SEM) images revealed that the samples consisted of hexagonal-shaped nanoplates with a different particle size distribution. Broad absorption bands assigned as transitions of $Ni^{2+}$ in oxygen octahedral sites were revealed by UV–vis spectra. Photoluminescence (PL) properties observed with a maximum peak centered in the blue-green region were attributed to different defects, which were produced during the nucleation process. We present a growth process scheme of the β-$Ni(OH)_2$ nanoplates.



## 1. Introduction

$Ni(OH)_2$ is widely used in many applications from power tools to portable electronics and electric vehicles [1] as well as a precursor for catalysts [2]. This material has a hexagonal layered structure with two polymorphs (α and β-$Ni(OH)_2$ ) [3–6]. The α-$Ni(OH)_2$ form is a hydroxyl-deficient phase with a hydrotalcite-like structure consisting of stacks of positively charged $Ni(OH)_{2-x}$ layers with intercalated anions and water molecules in the interlayer space to restore charge neutrality. The interlamellar distance is about 7.0 Å. The α-$Ni(OH)_2$ structure shows more disorderliness because the layers are randomly oriented. The β-form (a stoichiometric phase with a composition $Ni(OH)_2$) has a brucite-like structure with a hexagonal lattice consisting of an ordered stacking of well-oriented $Ni(OH)_2$ layers with no intercalated species in the interlayer space [7].

Various researches have been focused on the morphology-controllable preparation of $Ni(OH)_2$ and related composite materials [8–11]. The attention devoted to its shape is due to its important role in influencing magnetic, electrical, optical and other properties. There are many factors, which can affect product shapes; e.g., internal structure of the product, solvents used, temperature of the preparation, concentration of the reactants, use of surfactant templates, etc. [12–14]. The $Ni(OH)_2$ preparation method usually involves the precipitation of $Ni(OH)_2$ by employing an alkaline reagent such as urea, ammonia or sodium hydroxide [15–22]. Due to various methods used for the preparation of $Ni(OH)_2$, different morphologies such as nanosheets [22,23], nanotubes [24,25], nanorods [15], hollow spheres [26,27], stacks of pancakes [28] and carnation-like structures [29] have been obtained.

Microwave heat processing has been successfully applied for the preparation of microsized or nanosized inorganic materials [30–36]. The mechanism of energy transfer using a microwave field is very different from the mechanism of the three well-established modes of heat transfer; i.e., conduction, radiation and convection [37]. In particular, there is an interesting synthesis method utilizing reaction kinetics, which results in an increase in the reaction rate by one to two orders of magnitude, the formation of materials with different morphologies on a microscale or nanoscale, rapid heating, low synthesis temperatures, reduced processing times and low electrical energy costs; this method is environmentally friendly [38–41]. For this study, a β-$Ni(OH)_2$ nanostructure was prepared by a one-step MH synthesis from a nickel nitrate and aqueous ammonia precursor without the use of a template and other additives.

## 2. Experimental

Nickel hydroxide nanostructures were obtained using MH processing without the use of surfactants: 5.0 mmol of Nickel

* Corresponding author. Fax: +55 3432394143.
*E-mail addresses:* rclima@iqufu.ufu.br, renata@iq.unesp.br (R.C. Lima), elson@iq.unesp.br (E. Longo).

0022-4596/$ - see front matter © 2011 Elsevier Inc. All rights reserved.
doi:10.1016/j.jssc.2011.08.027

nitrate ($Ni(NO_3)_2 \cdot 6H_2O$) (99% purity, Aldrich) and 5.0 mL of ammonium hydroxide ($NH_4OH$) (30% in $NH_3$, Synth) were added to the solution until the pH value reached 12. This solution was placed in a conical flask with 80 mL of deionized water and stirred at room temperature for 15 min.

The solution was then transferred to a Teflon-lined stainless steel autoclave, sealed and placed in a MH domestic microwave (2.45 GHz), which was maintained at 100 °C for different times. A greenish product was separated by centrifugation, washed with deionized water and ethanol and dried at 60 °C in air.

The powders obtained were structurally characterized by XRD using a Rigaku-DMax/2500PC equipped with Cu$K\alpha$ radiation ($\lambda$=1.5406 Å) in the 2$\theta$ range from 10° to 100° with 0.02°/min. UV–vis spectroscopy of the crystalline sample powders was performed with Cary 5G equipment. The morphology was characterized by FE-SEM (Supra 35-VP, Carl Zeiss, Germany). The PL was measured with a Thermal Jarrel-Ash Monospec 27 monochromator and a Hamamatsu R446 photomultiplier. The 350.7 nm exciting wavelength of a krypton ion laser (Coherent Innova) was used, and the nominal output power of the laser was maintained at 550 mW. All measurements were taken at room temperature.

## 3. Results and discussion

Fig. 1 shows XRD patterns of samples processed by the MH method at 100 °C for 1, 8 and 32 min. XRD results revealed that all diffraction peaks can be indexed to the trigonal β-$Ni(OH)_2$ structure, which shows good agreement with the data reported in the literature (JCPDS card number 14-0117) [42]. The lattice parameters, $a=b=3.1298$ Å and $c=4.6106$ Å, and unit cell volume of 39.115 Å$^3$ were calculated using the least-square refinement from the UNITCELL-97 program [42,43]. The strong and sharp peaks indicate that the β-$Ni(OH)_2$ powders processed in MH are highly crystalline and structurally ordered at long range. These results show that the MH system promotes the complete crystallization of nickel hydroxide powders at low temperatures and reduced processing time. The peaks also indicate that the powders are free of secondary phases.

The Rietveld refinement of the β-$Ni(OH)_2$ sample obtained by the MH method at 100 °C for 1 min was performed using the GSAS program [44]. The diffraction peak profiles were further adjusted by the Thompson–Cox–Hastings pseudo-Voigt function and by an asymmetry function as described by Finger et al. [45]. The results obtained from the Rietveld refinement are presented

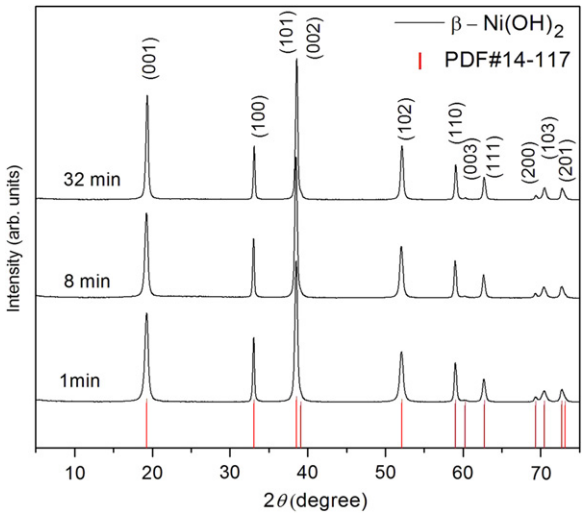


**Fig. 1.** XRD patterns of β-$Ni(OH)_2$ powders prepared by the MH method at 100 °C.

**Table 1**
Data from the Rietveld refinement of a β-$Ni(OH)_2$ powder processed by the MH method at 100 °C for 1 min.

| Space group | Lattice parameter (Å) | | Unit cell volume (Å$^3$) |
|---|---|---|---|
| $P-3m1$ | $a=b=3.1299$ | $c=4.6106$ | $V=39.116$ |

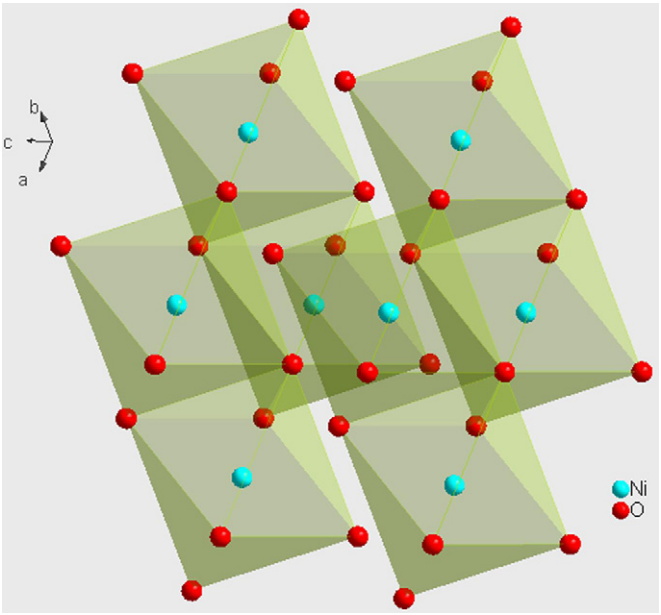


**Fig. 2.** Representation of a β-$Ni(OH)_2$ structure.

in Table 1. A schematic representation of the trigonal β-$Ni(OH)_2$ structure is shown in Fig. 2. The cell was constructed with structural parameters and atomic coordinates obtained from Rietveld refinement and shows the nickel atoms coordinated to four oxygen atoms in a planar square configuration.

The morphology of the β-$Ni(OH)_2$ powders prepared by the MH method at 100 °C for different reaction times was investigated using FE-SEM (see Fig. 3). These images reveal that the samples are irregular hexagonal shapes using 1 and 8 min processing time while the nanoplates obtained in 32 min exhibit regular hexagonal shapes with equal opposite edges. The micrographs show that the microwave irradiation contributes significantly to the formation of β-$Ni(OH)_2$ plates after short processing times.

Fig. 3 depicts nanoplates with different average particle distributions for samples obtained after treatment under hydrothermal conditions for 1, 8 and 32 min. Average size distributions of particle graphics were constructed from FE-SEM micrographs of β-$Ni(OH)_2$ plates using measurements of approximately 100 plates. The average particle sizes were 110, 115 and 146 nm for the samples treated under hydrothermal conditions for 1, 8 and 32 min, respectively. The particle sizes increase when the reaction time is increased.

In our synthetic strategy, nickel hydroxide was obtained by $Ni^{2+}$ hydrolysis in an aqueous solution. $Ni(NO_3)_2 \cdot 6H_2O$ was selected as the nickel source. An ammonia solution was employed as the coordinating agent, which reacts with $[Ni(H_2O)_6]^{2+}$ and controls the growth of β-$Ni(OH)_2$ nuclei.

Solid hydrated nickel (II) salts and their aqueous solutions usually contain a green $[Ni(H_2O)_6]^{2+}$ ion complex (see Fig. 4, step 1). In the presence of an excess of aqueous ammonia solution, the $[Ni(NH_3)_6]^{2+}$ stable species is formed, and the solution color changes

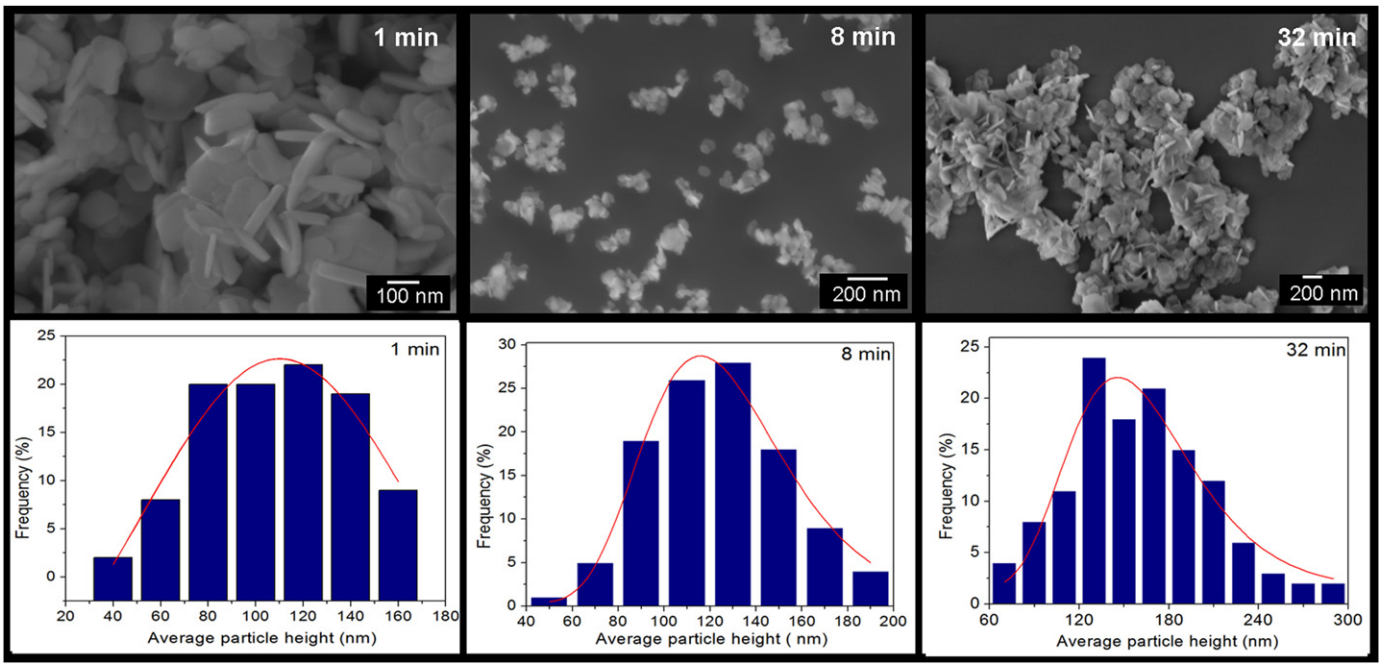


**Fig. 3.** FE-SEM images and particle average distributions of β-$Ni(OH)_2$ powders prepared by the MH method at 100 °C.

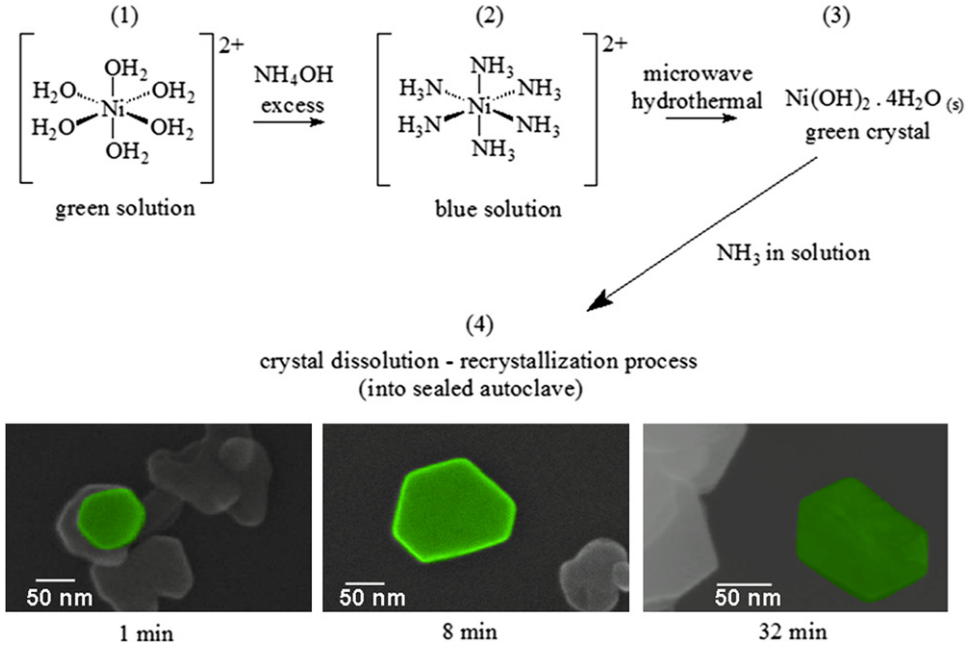


**Fig. 4.** Schematic representation of the growth process of $Ni(OH)_2$ nanoplates.

to blue (Fig. 4, step 2). In the presence of $Ni^{2+}$ and an $OH^-$ aqueous solution, the solution becomes turbid due to the formation of green $Ni(OH)_2$ precipitates. During MH treatment, the amount of green $Ni(OH)_2$ crystal precipitates increases (see Fig. 4, step 3).

Fig. 3 shows the low-magnification FE-SEM images of nanoplates, which indicate that the interaction between the $NH_3$ and nanoplates plays an important role in the 2D pattern population. In a polar solvent ($H_2O$–$NH_3$), the dipole moments are larger, so they have stronger dipole–dipole interactions between the nanocrystals. The dipole–dipole interactions may cause the nanocrystals to favor growth in a particular direction. Solvent polarity promotes faster growth of nanocrystals along a particular direction, which results in nanoplates with a two-dimensional configuration. FE-SEM images (Figs. 3 and 4) verify that the nanoplates are assemblies of small crystals rather than single crystal. Density functional calculations [46–48] reveal that growth is an order–disorder–order pattern of a cyclic nature. Growth proceeds via disordered clusters between two ordered clusters, and global order emerges rapidly with the addition of only one or two atoms.

From FE-SEM analyses, we concluded that the morphologies can be obtained via a crystallization–dissolution–recrystallization self-assembly growth mechanism (Fig. 4, step 4) [37,49]. This process occurs in a sealed hydrothermal system during 1, 8 and

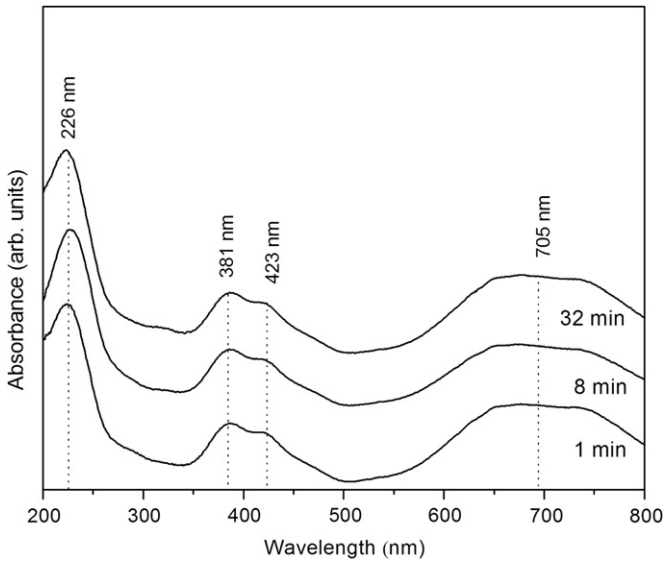


**Fig. 5.** UV–vis absorbance spectra of β-Ni(OH)$_2$ powders prepared by the MH method at 100 °C.

32 min of reaction time and results in different shapes. When the reaction time was increased to 32 min, the product was composed of plate-like nanostructures with a regular hexagonal shape. A growth process scheme of Ni(OH)$_2$ nanoplates is presented in Fig. 4.

During the growth process, large amounts of nuclei are first generated, and then they expand into primary nanoparticles, which are active; a number of them will orient and assemble into a large nanocrystal. However, the assembly process may also produce defects in the crystals obtained, and therefore parts of the nanocrystals are more easily decomposable. When the blue solution Ni(NH$_3$)$_6$ was treated under hydrothermal conditions for 1, 8 and 32 min, a multicrystal assembled porous structure formed (an aggregate crystal), which may create a new opportunity to facilitate the application of nickel hydroxide-based nanocrystals. This kind of aggregate is a special case of colloidal crystals, which can create materials with complex structures. Self-alignment crystal assemblies of semiconductors of this variety may also bring new electronic and optical properties to materials.

Fig. 5 shows β-Ni(OH)$_2$ optical absorption characteristics in the UV and visible region. The β-Ni(OH)$_2$ is characterized by a sharp peak at 226 nm; this absorption in the UV region is attributed to band gap absorptions in β-Ni(OH)$_2$ of about 4.4 eV. The optical band gap energy can be estimated using the equation proposed by Wood and Tauc [50]. Absorption spectra exhibit three other broad bands at 381, 423 and 705 nm. These β-Ni(OH)$_2$ absorption bands were assigned as transitions of $Ni^{2+}$ in oxygen octahedral sites from the ground state $^3A_{2g}$ to $^3T_{2g}(G)$, $^3A_{2g}$ to $^3T_{1g}(P)$ and $^3A_{2g}$ to $^3T_{1g}(F)$ states [51,52].

PL spectra recorded at room temperature for β-Ni(OH)$_2$ samples obtained by MH processing for 1, 8 and 32 min at 100 °C are shown in Fig. 6.

Both surface states and lattice defects are closely related to crystal growth mechanisms. Recently, it was observed that the nucleation and growth processes are related to the size and distribution of the defects and that the luminescence mechanism of defects varies during different synthesis time [46]. However, most of the research for improving the quantum yield is still based on the assumption that the classic Oswald ripening (OR) growth mechanism is involved in the liquid-phase synthesis of nanocrystals, which are inclined to have relatively internal lattices where the variation of the bulk and surface defects is the main factor influencing luminescent properties [47].

The above phenomena are illustrated in Fig. 6. The strong defect induced luminescence of the initial nanoparticles can be attributed mainly to complex cluster vacancies that arise from fast crystallization during the initial nucleation process. At the beginning of OR growth, these defects could be concentrated in the nanocrystals.

These factors result in different structural defects such as oxygen vacancies and bond distortions, which can promote the formation of intermediary energy levels within the band gap. The profile of the emission band is typical of a multiphonon process; i.e., a system in which relaxation occurs by several paths involving the participation of numerous states within the material band gap. This behavior is associated with the structural disorderliness of material and indicates the presence of additional electronic levels in the forbidden band gap of the material [48,53]. The general aspect of the spectra is a broad band covering a large part of the visible spectra with one dominant maximum emission centered at blue emission.

Based on the Gaussian line broadening mechanism for luminescence processes [52,54], PL curves were decomposed into five components (see Fig. 6). The peaks correspond to the blue-green region in the visible spectrum where its maximum peak intensity appears at about 455.8, 459.6 and 454.7 nm in 1, 8 and 32 min of processing time, respectively. Each component represents a different type of electronic transition, which can be linked to the structural arrangement or surface defects. The parameters obtained in the fit are recorded in Table 2, including the individual position, area and amplitude of each peak.

Theoretical results verify that a breaking symmetry process in the structure of various semiconductors associated with order–disorder effects is a necessary condition for intermediate levels in the forbidden band gap [46–48,55,56]. These structural changes can be related to the charge polarization in different ranges that, at the very least, are manifestations of quantum confinement when they occur at short and intermediate ranges independent of the particle size. The main point for quantum confinement is discrete levels in the band gap, which is impossible with periodic crystals or defects.

Cluster-to-cluster charge transfer (CCCT) for a crystal with more than one type of cluster is defined to be an excitation transition of an electron from one cluster to the other.

The structural and electronic reconstruction of all the possible combinations of clusters in a crystal is essential to understand the CCCT process and the PL phenomenon. In this case, a decrease in the band gap and possibly the surface leads to the dislocation of the natural nickel hydroxide green emission to the blue emission. Photo-induced electron transfers exist where an electron is promoted from an occupied level of the cluster donor to a vacant level of the cluster receptor.

## 4. Summary

Crystalline nickel hydroxide nanostructures were successfully prepared using the MH method at low temperatures and short reaction times. The trigonal β-Ni(OH)$_2$ phase and transitions of $Ni^{2+}$ in oxygen octahedral sites were detected by XRD and UV–vis analyses, respectively. The growth process of crystals during MH conditions plays an important role in the formation of β-Ni(OH)$_2$ nanoplates. The emission luminescence observed with excitation in the UV–vis range was used as a tool for the study of the structure. The maximum PL emission appears at about 456 nm in the blue-green region of the visible spectrum. Aqueous ammonia was used as a precursor to provide hydroxyl ions for the

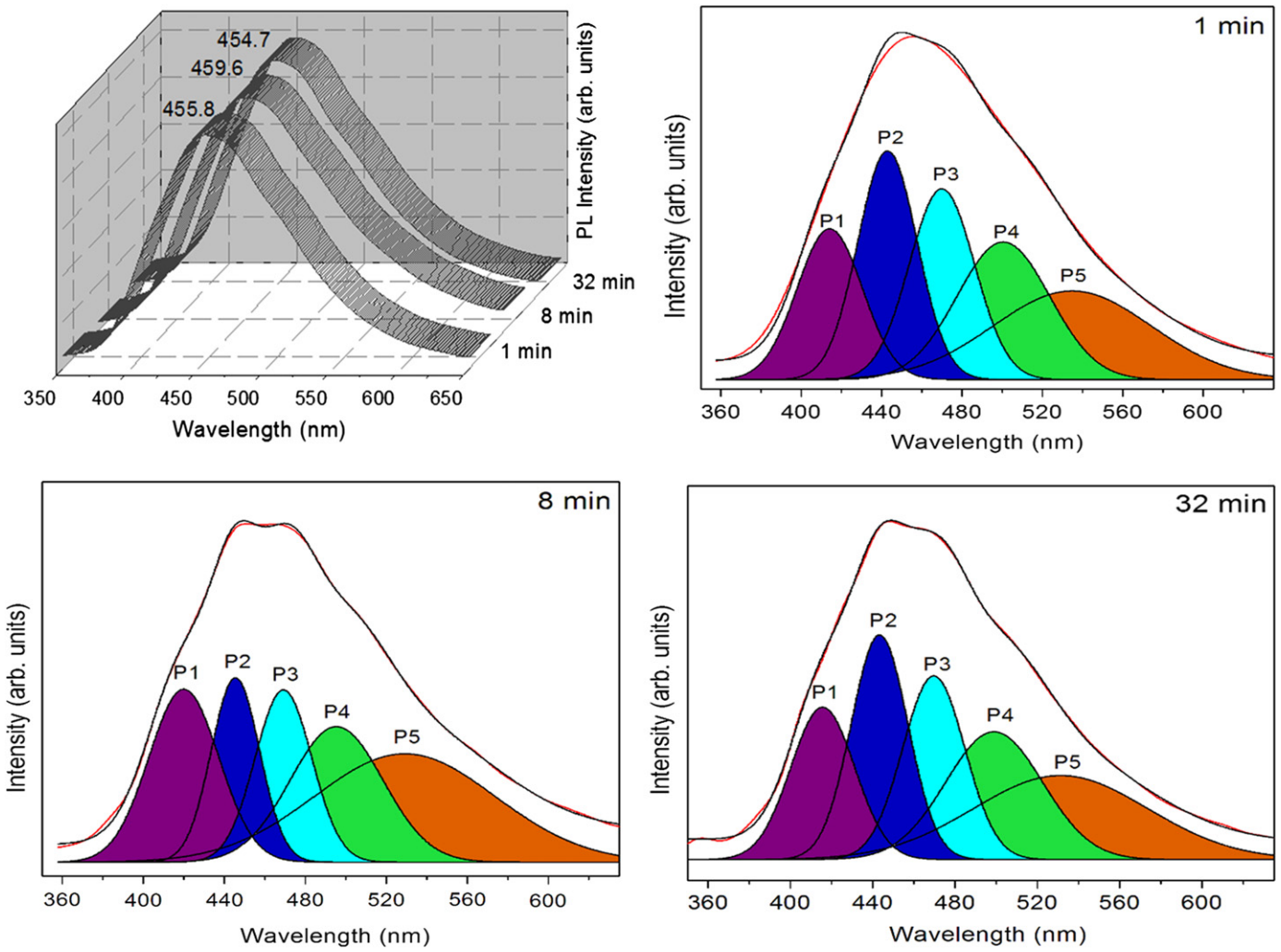


**Fig. 6.** PL spectra at room temperature of β-Ni(OH)$_2$ powders prepared by the MH method at 100 °C.

**Table 2**
Data obtained from the decomposition of PL curves of β-Ni(OH)$_2$ powders processed by the MH method at 100 °C.

| **Processing time** | **1 min** | | **8 min** | | **32 min** | |
|---|---|---|---|---|---|---|
| **Center of maximum PL emission** | 455.8 nm | | 459.6 nm | | 454.7 nm | |
| **Parameters** | λ (nm) | Area (%) | λ (nm) | Area (%) | λ (nm) | Area (%) |
| Peak-$P_1$ | 414.1 | 15.7 | 419.9 | 19.5 | 415.6 | 15.9 |
| Peak-$P_2$ | 442.0 | 21.6 | 445.4 | 14.1 | 443.3 | 20.8 |
| Peak-$P_3$ | 469.0 | 19.9 | 469.1 | 15.5 | 469.6 | 18.7 |
| Peak-$P_4$ | 500.5 | 20.4 | 495.4 | 20.0 | 498.9 | 20.3 |
| Peak-$P_5$ | 534.3 | 22.3 | 528.1 | 30.9 | 531.0 | 24.0 |

formation of β-Ni(OH)$_2$. $[Ni(NH_3)_6]^{2+}$ complex ions, which are formed in liquid-phase and may control the reaction rate of $Ni^{2+}$ ions with $OH^-$ ions for the formation of β-Ni(OH)$_2$ regular nanoplate structures.

## Acknowledgments

The authors are grateful for the support of the Brazilian research financing institutions: CAPES, CNPq, FAPESP and INCTMN. They also thank Rorivaldo Camargo and Madalena Tursi for technical support.

## References

[1] L.X. Yanga, Y.J. Zhua, H. Tonga, Z.H. Lianga, L. Lia, L. Zhanga, J. Solid State Chem. 180 (2007) 2095–2101.
[2] S. Ovshinsky, M.A. Feteenko, J. Ross, Science 260 (1993) 176–181.
[3] C. Coudun, F. Grillon, J.F. Hochepied, Colloids Surf. A 280 (2006) 23–31.
[4] S. Sarkar, M. Pradhan, A.K. Sinha, M. Basu, Y. Negishi, T. Pal, J. Inorg. Chem. 49 (2010) 8813–8827.
[5] B. Mavis, M. Akinc, Chem. Mater. 18 (2006) 5317–5325.
[6] P. Jeevanandam, Y. Koltypin, A. Gedanken, Nano Lett. 1 (2001) 263–266.
[7] L.P. Xu, Y.S. Ding, C.H. Chen, L.L. Zhao, C. Rimkus, R. Joesten, S.L. Suib, Chem. Mater. 20 (2008) 308–316.
[8] B. Liu, X.Y. Wang, H.T. Yuan, Y.S. Zhang, D.Y. Song, Z.X. Zhou, J. Appl. Electrochem. 29 (1999) 855–860.
[9] I.J. Zhitomirsky, J. Appl. Electrochem. 34 (2004) 235–240.
[10] W.K. Hu, X.P. Gao, M.M. Geng, Z.X. Gong, D. Noreus, J. Phys. Chem. B 109 (2005) 5392–5394.
[11] W.Y. Li, S.Y. Zhang, J. Chen, J. Phys. Chem. B 109 (2005) 14025–14032.
[12] X.L. Li, J.F. Liu, Y.D. Li, Mater. Chem. Phys. 80 (2003) 222–227.
[13] X. Liu, Y. Lan, Mater. Lett. 58 (2004) 1327–1330.
[14] X.H. Liu, G.Z. Qiu, Z. Wang, X.G. Li, Nanotechnology 16 (2005) 1400–1405.
[15] K. Matsui, T. Kyotani, A. Tomita, Adv. Mater. 14 (2002) 1216–1219.
[16] F.S. Cai, G.Y. Zhang, J. Chen, X.L. Gou, H.K. Liu, S.X. Dou, Angew. Chem. Int. Ed. 43 (2004) 4212–4216.
[17] S.L. Chou, F.Y. Cheng, J. Chen, Eur. J. Inorg. Chem. 20 (2005) 4035–4039.
[18] D.N. Yang, R.M. Wang, M.S. He, J. Zhang, Z.F. Liu, J. Phys. Chem. B 109 (2005) 7654–7658.
[19] D.N. Yang, R.M. Wang, J. Zhang, Z.F. Liu, J. Phys. Chem. B 108 (2004) 7531–7533.
[20] M. Akinc, N. Jongen, J. Lemaitre, H. Hofmann, J. Eur. Ceram. Soc. 18 (1998) 1559–1564.
[21] B. Cheng, Y. Le, W. Cai, J. Yu, J. Hazard. Mater. 185 (2011) 889–897.
[22] Z.H. Liang, Y.J. Zhu, X.L. Hu, J. Phys. Chem. B 108 (2004) 3488–3491.

[23] D.L. Chen, L. Gao, Chem. Phys. Lett. 405 (2005) 159–164.
[24] X.H. Li, L.Y. Zhang, Z.P. Bai, J.J. Zhu, J. Nanosci. Nanotechnol. 10 (2010) 5191–5195.
[25] Q.-Z. Jiao, Z.-L. Tian, Y. Zhao, J. Nanopart. Res. 9 (2007) 519–522.
[26] Y. Wang, Q.S. Zhu, H.G. Zhang, Chem. Commun. (2005) 5231–5233.
[27] D.B. Wang, C.X. Song, Z.S. Hu, X. Fu, J. Phys. Chem. B 109 (2005) 1125–1129.
[28] C. Coudun, J.F. Hochepied, J. Phys. Chem. B 109 (2005) 6069–6074.
[29] L.X. Yang, Y.J. Zhu, H. Tong, Z.H. Liang, W.W. Wang, Cryst. Growth Des. 7 (2007) 2716–2719.
[30] M.L. Santos, R.C. Lima, C.S. Riccardi, R.L. Tranquilin, P.R. Bueno, J.A. Varela, E. Longo, Mater. Lett. 62 (2008) 4509–4511.
[31] R.C. Lima, L.R. Macario, J.W.M. Espinosa, V.M. Longo, R. Erlo, N.L. Marana, J.R. Sambrano, M.L.D. Santos, A.P. Moura, P.S. Pizani, J. Andrès, E. Longo, J.A. Varela, J. Phys. Chem. A 112 (2008) 8970–8978.
[32] P. Benito, M. Herrero, C. Barriga, F.M. Labajos, V. Rives, Inorg. Chem. 47 (2008) 5453–5463.
[33] F.V. Motta, R.C. Lima, A.P.A. Marques, M.S. Li, E.R. Leite, J.A. Varela, E. Longo, J. Alloys Compd. 497 (2010) L25–L28.
[34] C.S. Riccardi, R.C. Lima, M.L.D. Santos, P.R. Bueno, J.A. Varela, E. Longo, Solid State Ionics 180 (2009) 288–291.
[35] A.P. Moura, L.S. Cavalcante, J.C. Sczancoski, D.G. Stroppa, E.C. Paris, A.J. Ramirez, J.A. Varela, E. Longo, Adv. Powder Technol. 21 (2010) 197–202.
[36] A.P. de Moura, R.C. Lima, M.L. Moreira, D.P. Volanti, J.W.M. Espinosa, M.O. Orlandi, P.S. Pizani, J.A. Varela, E. Longo, Solid State Ionics 181 (2010) 775–780.
[37] T.L. Lai, Y.Y. Shu, G.L. Huang, C.C. Lee, C.B. Wang, J. Alloys Compd. 450 (2008) 318–322.
[38] S. Komarneni, M.C. D'Arrigo, C. Leonelli, G.C. Pellacani, H. Katsuki, J. Am. Ceram. Soc. 81 (1998) 3041–3043.
[39] S. Komarneni, R.K. Rajha, H. Katsuki, Mater. Chem. Phys. 61 (1999) 50–54.
[40] D. Keyson, D.P. Volanti, L.S. Cavalcante, A.Z. Simoes, I.A. Souza, J.S. Vasconcelos, J.A. Varela, E. Longo, J. Mater. Process. Technol. 189 (2007) 316–319.
[41] M. Godinho, C. Ribeiro, E. Longo, E.R. Leite, Cryst. Growth Des. 8 (2008) 384–386.
[42] T.J.B. Holland, S.A.T. Redfern, Mineral. Mag. 61 (1997) 65–77.
[43] D.B. Kuang, B.X. Lei, Y.P. Pan, X.Y. Yu, C.Y. Su, J. Phys. Chem. C 113 (2009) 5508–5513.
[44] A.C. Larson, R.B. Von Dreele, GSAS—General Structure Analysis System, Los Alamos National Laboratory, EUA, 2001, pp. 86–748.
[45] L.W. Finger, D.E. Cox, A.P. Jephcoat, J. Appl. Crystallogr. 27 (1994) 892–900.
[46] M.L. Moreira, G.P. Mambrini, D.P. Volanti, E.R. Leite, M.O. Orlandi, P.S. Pizani, V.R. Mastelaro, C.O. Paiva-Santos, E. Longo, J.A. Varela, Chem. Mater. 20 (2008) 5381–5387.
[47] V.M. Longo, L.S. Cavalcante, R. Erlo, V.R. Mastelaro, A.T. de Figueiredo, J.R. Sambrano, S. de Lazaro, A.Z. Freitas, L. Gomes, N.D. Vieira, J.A. Varela, E. Longo, Acta Mater. 56 (2008) 2191–2202.
[48] V.M. Longo, L.S. Cavalcante, A.T. de Figueiredo, L.P.S. Santos, E. Longo, J.A. Varela, J.R. Sambrano, C.A. Paskocimas, F.S. De Vicente, A.C. Hernandes, Appl. Phys. Lett. 90 (2007) 091906-1–091906-3.
[49] Z.J. Luo, H.M. Li, H.M. Shu, K. Wang, J.X. Xia, Y.S. Yan, Cryst. Growth Des. 8 (2008) 2275–2281.
[50] D.L. Wood, J. Tauc, J. Phys. Rev. B 5 (1972) 3144–3151.
[51] Y. Qi, H. Qi, J. Li, C. Lu, J. Cryst. Growth 310 (2008) 4221–4225.
[52] G.R. Rossman, R.D. Shannon, R.K. Waring, J. Solid State Chem. 39 (1981) 277–287.
[53] E.A.V. Ferri, J.C. Sczancoski, L.S. Cavalcante, E.C. Paris, J.W.M. Espinosa, A.T. de Figueiredo, P.S. Pizani, V.R. Mastelaro, J.A. Varela, E. Longo, Mater. Chem. Phys. 117 (2009) 192–198.
[54] T. Ding, W.T. Zheng, H.W. Tian, J.F. Zang, Z.D. Zhao, S.S. Yu, X.T. Li, F.L. Meng, Y.M. Wanga, X.G. Kong, Solid State Commun. 132 (2004) 815–819.
[55] E. Cavalli, P. Boutinaud, R. Mahiou, M. Bettinelli, P. Dorenbos, Inorg. Chem. 49 (2010) 4916–4921.
[56] S.K. Arora, B. Chudasama, Cryst. Res. Technol. 41 (2006) 1089–1095.